Adv. Polar Upper Atmos. Res., 13, 37-47, 1999

STATISTICAL ANALYSIS OF ECHO POWER, DOPPLER VELOCITY AND SPECTRAL WIDTH OBTAINED WITH THE SYOWA SOUTH HF RADAR

Masaaki FUKUMOTO[1], Nozomu NISHITANI[1], Tadahiko OGAWA[1], Natsuo SATO[2], Hisao YAMAGISHI[2] and Akira Sessai YUKIMATU[2]

[1] *Solar-Terrestrial Environment Laboratory, Nagoya University, Honohara, Toyokawa 442-8507*
[2] *National Institute of Polar Research, Kaga 1-chome, Itabashi-ku, Tokyo 173-8515*

Abstract: Statistical analyses are made of the physical parameters (echo power, Doppler velocity and spectral width) of Doppler spectra obtained in September 1995 with the Syowa South HF radar. We present time and range distributions and histograms of the parameters and cross-correlations among them. With K index at Syowa Station the distributions and histograms vary slightly but the correlations do not change so much. The most noticeable feature is that there is a positive correlation between the absolute values of Doppler velocity and echo power. This relationship can be interpreted in terms of the gradient-drift instability which is the most probable cause to generate decameter-scale irregularities in the F-region ionosphere.

1. Introduction

An HF radar can measure echoes backscattered from E and F region irregularities (*e.g.*, GREENWALD *et al.*, 1985). From a Doppler spectrum of echoes, we obtain three kinds of parameters (echo power, Doppler velocity and spectral width). Echo power is a scattered echo intensity and is defined as a ratio to background noise (S/N ratio). Doppler velocity corresponds to line-of-sight plasma velocity. Spectral width gives temporal and spatial variability of the irregularities responsible for backscattering.

Previous studies using VHF and HF radars at high latitudes have revealed various kinds of physical properties of the E-region ionosphere. For example, OGAWA and IGARASHI (1982), using a 50 MHz radar at Syowa Station, found that with increasing electric field, echo power and Doppler velocity increase and Doppler spectrum changes from a diffuse form to a discrete form (two-stream-like spectrum). HANUISE *et al.* (1991) made statistical study of the E-region Doppler spectra obtained with the SHERPA HF radar in Canada to discuss the three parameters and the correlation between them. They found that the ionospheric echoes from the E-region have two kinds of origins, two-stream and gradient-drift plasma waves. In contrast, only a few statistical studies have been made for F-region echoes. ROUHONIEMI and GREENWALD (1996, 1997) have studied statistical distributions of Doppler velocity and echo power; however, analysis of the correlations among the parameters was not presented.

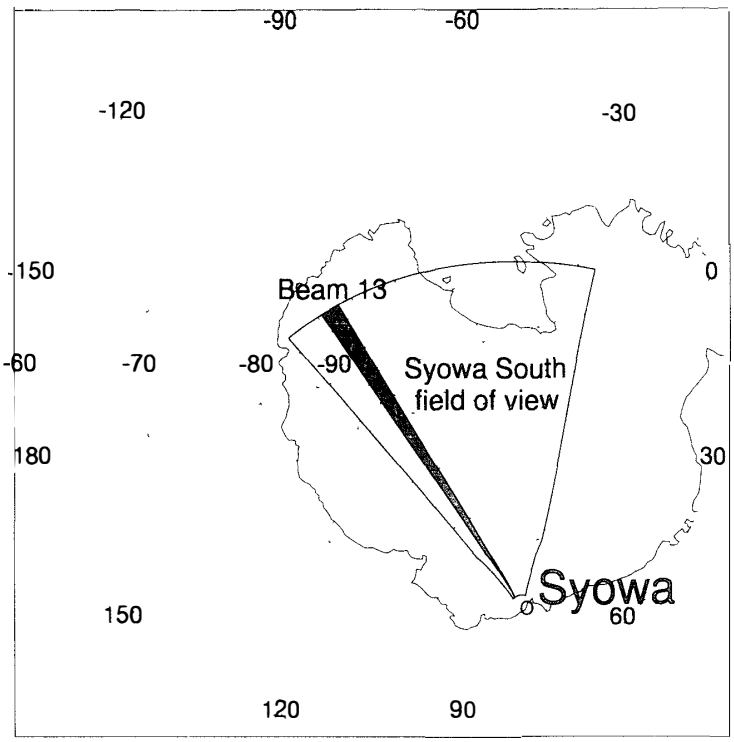

Fig. 1. Field of view of the Syowa South HF radar in geomagnetic coordinates. Data used in this paper are obtained with beam 13.

In this study, we present statistical analyses of the parameters obtained with the Syowa South HF radar and discuss physical characteristics of the *F*-region irregularities at high latitudes and in the polar cap.

2. Results

2.1. Data

Figure 1 shows the field of view of the Syowa South HF radar. Magnetic local time (MLT) at Syowa Station is approximately the same as universal time (UT). Data used in this paper were obtained on beam 13 which is aligned in the magnetic north-south direction. Spatial and temporal resolution of the radar are $\simeq$45 km and $\simeq$2 min, respectively. We use the data for the period of September 1995 when echo reception conditions were good. Data (echo power, Doppler velocity and spectral width) were processed from the original raw-format file by using the fitacf program (version 2.42).

In our analysis, data which have Doppler velocity within $\pm$60 m/s as well as spectral width less than 60 m/s are excluded as ground scatter echoes. In addition, data satisfying at least one of the following criteria are eliminated as 'bad' data; 1) echo power below 0 dB or above 30 dB, 2) Doppler velocity beyond $\pm$1000 m/s, or 3) spectral width above 1000 m/s. Moreover, in order to exclude noise and radio interference, we limit data to be analyzed as follows: 1) Echoes detected at three consecutive range intervals (~90 km) for more than two radar scans (~2 min), and 2) Echoes with

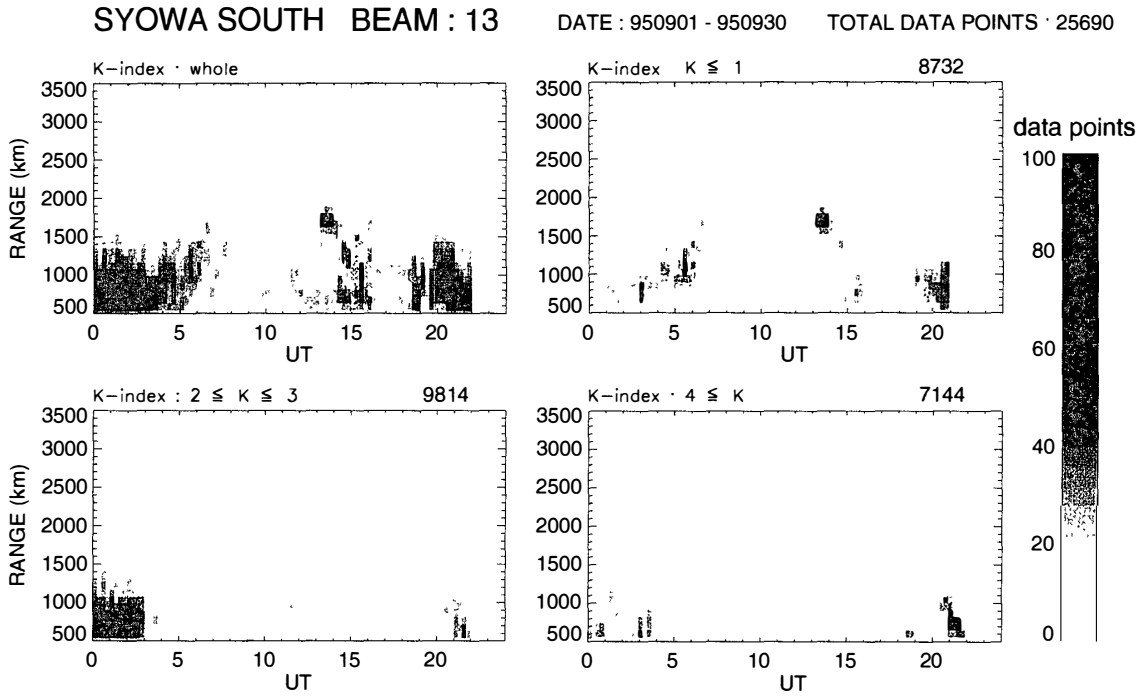

Fig. 2. Distribution of data points as a function of universal time and range. MLT at Syowa Station is approximately the same as UT. Upper left panel exhibits the data for whole geomagnetic activity, and other panels are for quiet (K indices at Syowa Station range from 0 to 1), moderately disturbed ($2 \leq K \geq 3$) and highly disturbed ($K \geq 4$) periods.

Doppler velocities increasing or decreasing monotonically at three consecutive range intervals, or echoes with relatively small difference ($\leq 33\%$) in Doppler velocity as compared to the adjacent range.

Figure 2 shows distributions of the data as a function of universal time and radar range. In order to exclude echoes from the *E*-region, we limit the range to beyond 500 km. Upper left panel exhibits the data for all geomagnetic activities, and other panels are for quiet (*K* indices at Syowa Station ranging from 0 to 1), moderately disturbed ($2 \leq K \leq 3$) and highly disturbed ($K \geq 4$) periods. The data points are strongly concentrated in the nightside sector at range of 500 km to 1000 km. This is probably due to the sunlight which reduces echoes (that is, decameter-irregularity production) in the dayside hours and to the decrease of backscattered echoes with distance. There is lack of data at 0900–1200 UT for $K \geq 4$. The lack of data at 2200–2400 UT in all the panels is due to no radar operation.

2.2. *Statistical analysis of parameters*

Figure 3 shows polar plots of the echo power distribution. There are strong-echo regions around noon and midnight which are related to the cusp and highest auroral activity region, respectively (*e.g.*, RUOHONIEMI and GREENWALD, 1997). Histograms of the echo power are plotted in Fig. 4. The decreases in relative echo number below 7 dB is partly due to our technique to eliminate ground scatter and noises. The three histograms ($K \leq 1$, $2 \leq K \leq 3$ and $4 \leq K$) show a similar shape, but the distribution for

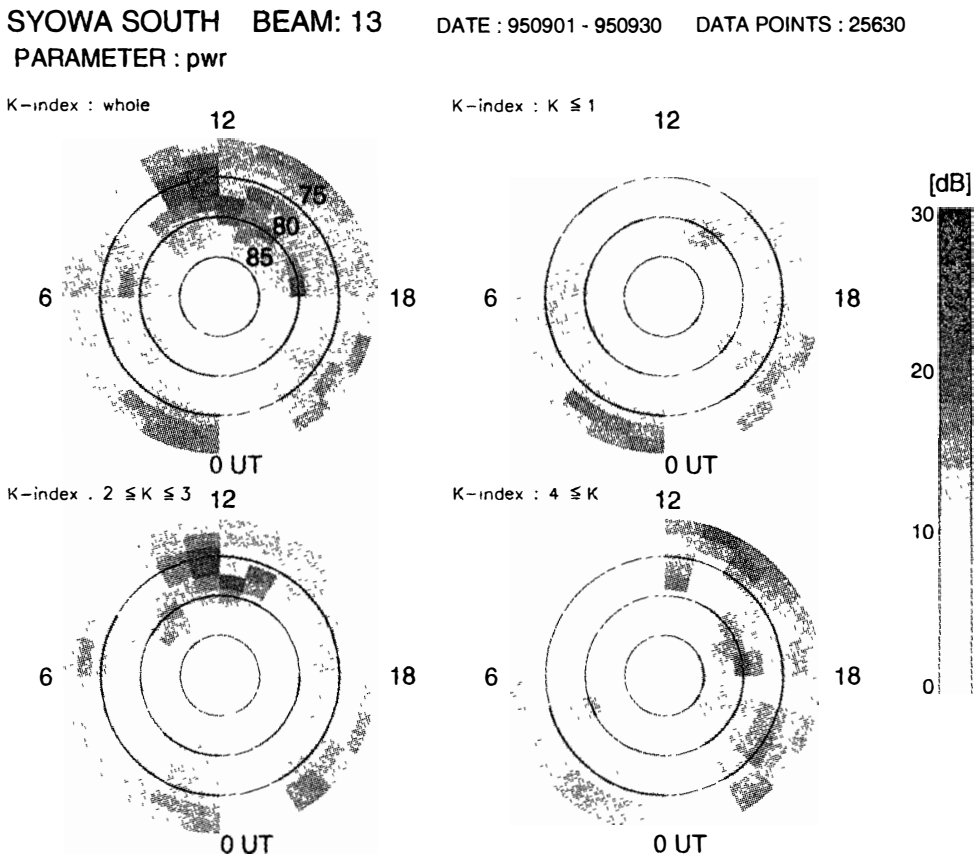

Fig. 3. Polar plots of echo power for four geomagnetic activity levels. Data points are classified in the same way as in Fig. 2. Solid circles in each panel show geomagnetic latitudes of 75, 80 and 85 degrees.

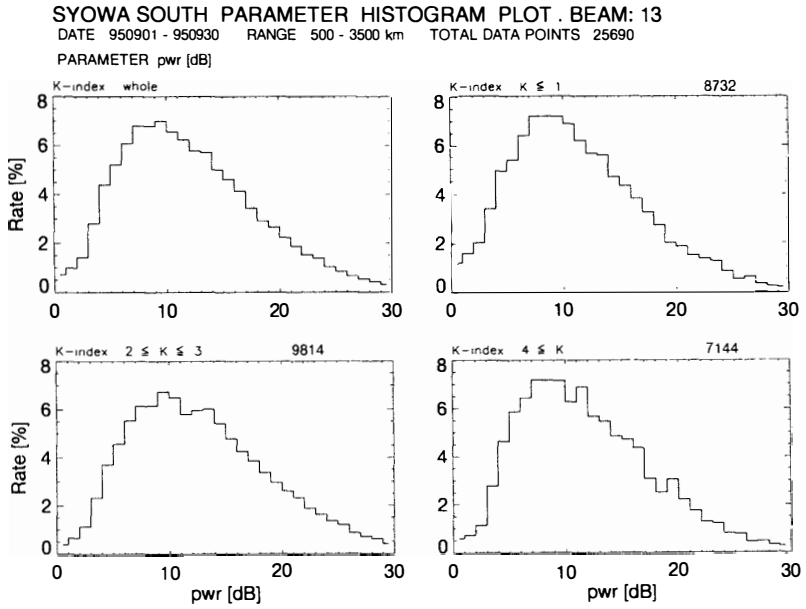

Fig. 4. Histograms of echo power for four geomagnetic activity levels. Decrease in the relative number of data points at lower power is due to elimination of ground scatter, noise and interference.

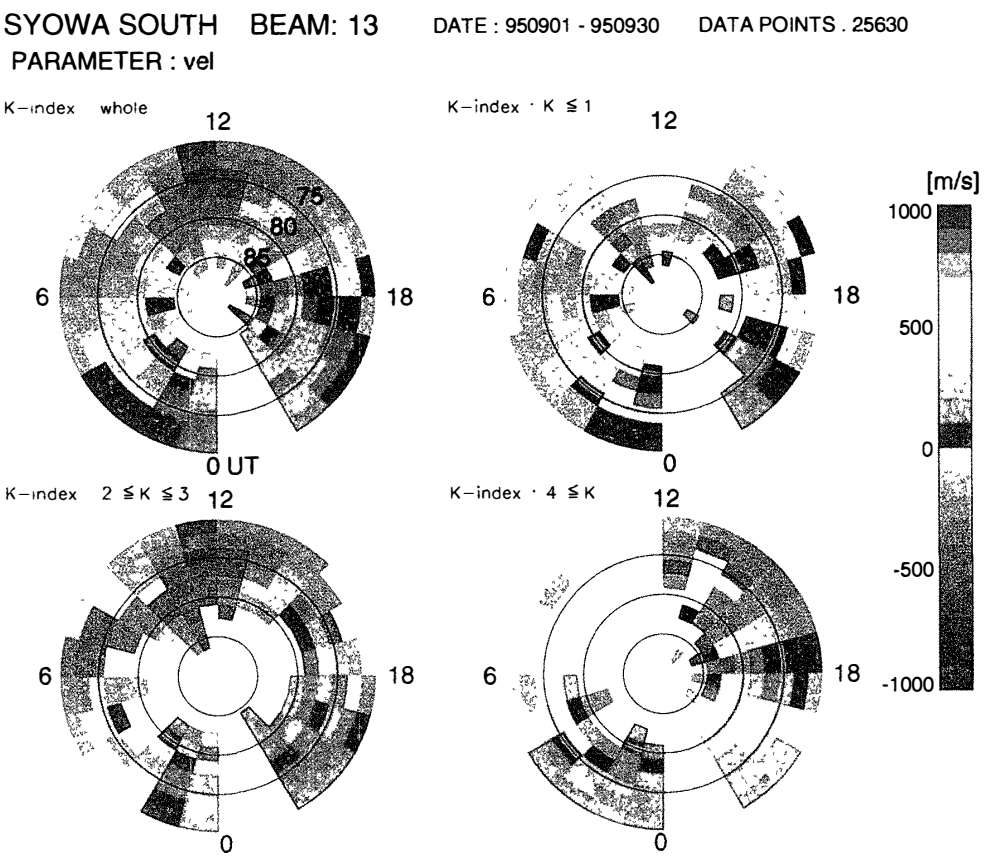

Fig. 5. Polar plots of Doppler velocity for four geomagnetic activity levels.

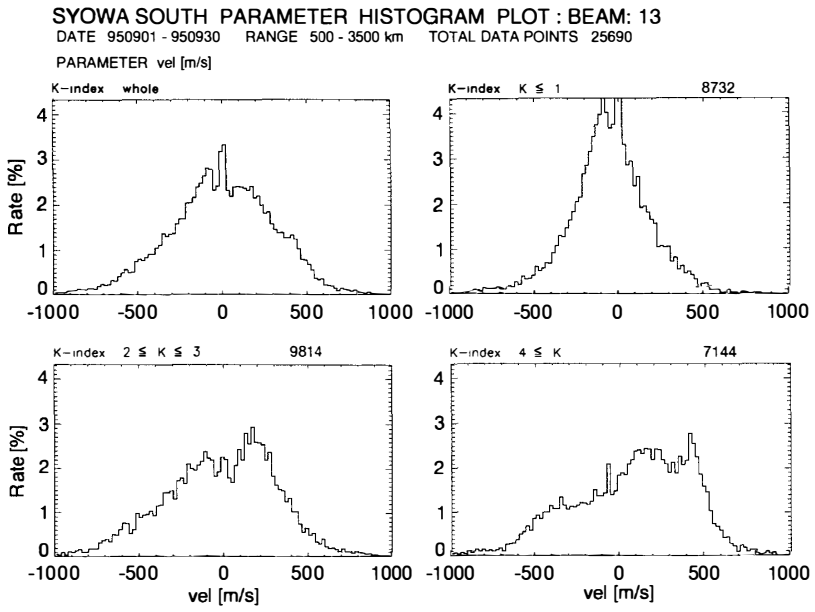

Fig. 6. Histograms of Doppler velocity for four geomagnetic activity levels.

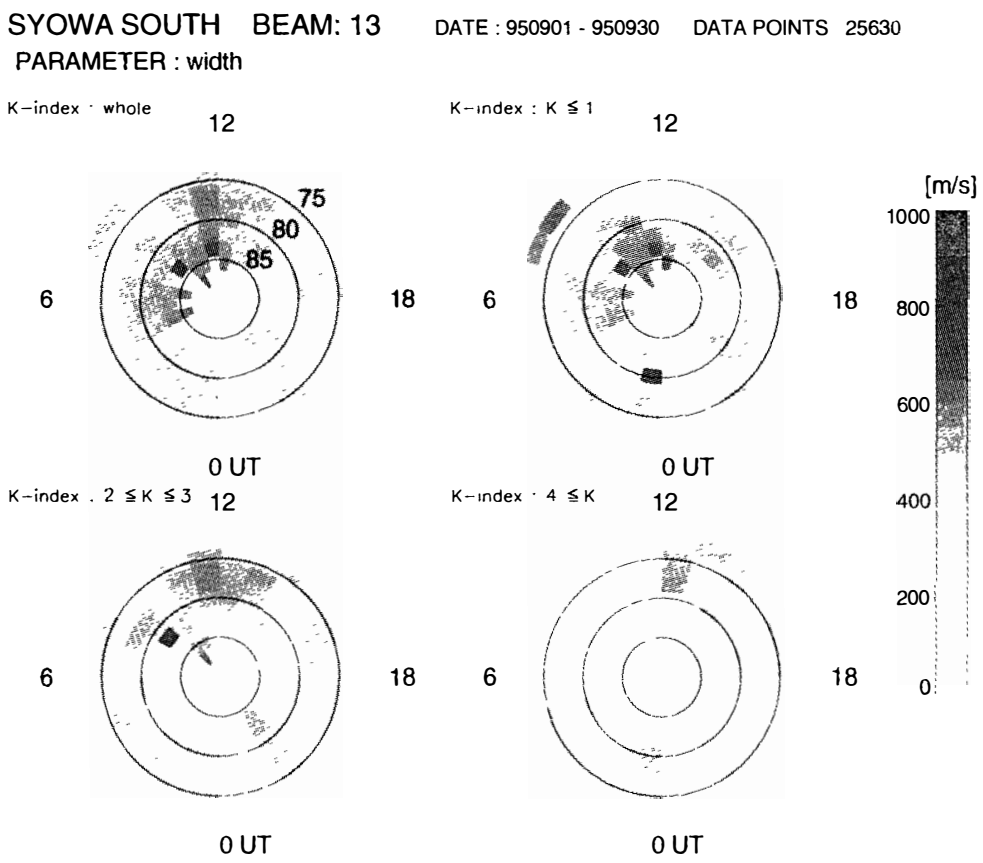

Fig. 7. Polar plots of spectral width for four geomagnetic activity levels.

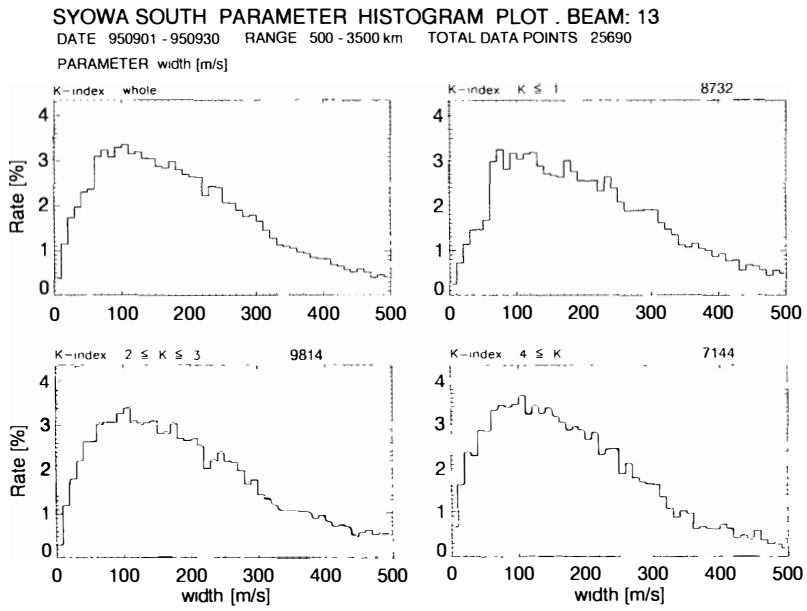

Fig. 8. Histograms of spectral width for four geomagnetic activity levels. Decrease in the relative number of data points below 60 m/s is due to elimination of ground scatter.

$2 \leq K \leq 3$ is slightly different from the others; relative numbers of echoes below 10 dB are smaller and those above 13 dB are larger than the others.

Figure 5 shows polar plots of the line-of-sight Doppler velocity distribution. Equatorward (northward) velocities are taken positive and poleward (southward) velocities negative. Basically, Doppler velocity is negative on the dayside and positive on the nightside. These senses of velocity are consistent with the two-cell plasma convection pattern (HEPPNER and MAYNARD, 1987). The locations of the boundary between poleward and equatorward velocity vary with increasing K index; the region with positive velocity spreads with increasing K index and the post-midnight sector (0200–0400 UT) tends to show poleward plasma velocity for quiet to moderately disturbed period. Histograms of the Doppler velocity are shown in Fig. 6. The relative number of higher-velocity echoes increases with geomagnetic activity (NISHITANI *et al.*, 1997). A noticeable asymmetry of the histogram for $K \geq 4$ is due to the biased MLT distribution of data points shown in Fig. 2; note the data lack at 09–12 UT.

Figure 7 shows polar plots of the spectral width. There are regions with greater spectral widths (≥ 400 m/s) around noon, probably being related to cusp precipitations (*e.g.*, BAKER *et al.*, 1995). Histograms of the spectral width are plotted in Fig. 8. These histograms are similar to each other but the peak at about 100 m/s becomes more obvious with increasing K index. Again the decreases of relative echo number below 60 m/s are due to our technique for eliminating ground scatter and noises.

2.3. Correlation between parameters

In Fig. 9, we show scatter plots of the echo power as a function of Doppler velocity. The solid curve with standard deviations shows the averaged echo power in each Doppler velocity bin. It is noticeable that in all panels there is a positive correlation between the absolute value of Doppler velocity and echo power. The echo power increases with increasing Doppler velocity up to ± 500 m/s (there are not enough data points for velocities beyond ± 500 m/s, as already indicated in Fig. 6, so the relationship in these areas should be ignored). This fact can be interpreted in terms of the gradient-drift instability which is the most probable cause for generating decameter-scale irregularities in the F-region (*e.g.*, TSUNODA, 1988). Detailed discussion is given in the following section.

Scatter plots of the spectral width as a function of Doppler velocity is shown in Fig. 10. The solid curves with standard deviations show the average width in each velocity bin. There are not enough data points for velocities beyond ± 500 m/s. There are no data at small velocity ($\leq \pm 60$ m/s) and small width (≤ 60 m/s) due to our technique for eliminating ground scatter. Since a spectral width reflects spatial and temporal variability of Doppler velocity in each radar range bin, spectral width is expected to increase with the absolute value of Doppler velocity. The data with negative Doppler velocity in Fig. 10 are consistent with this expectation. On the other hand, the spectral width does not increase with positive velocity. To understand this behavior, more detailed analysis is necessary. Discussion of this correlation is also given in the following section.

Scatter plots of the echo power as a function of spectral width are shown in Fig.

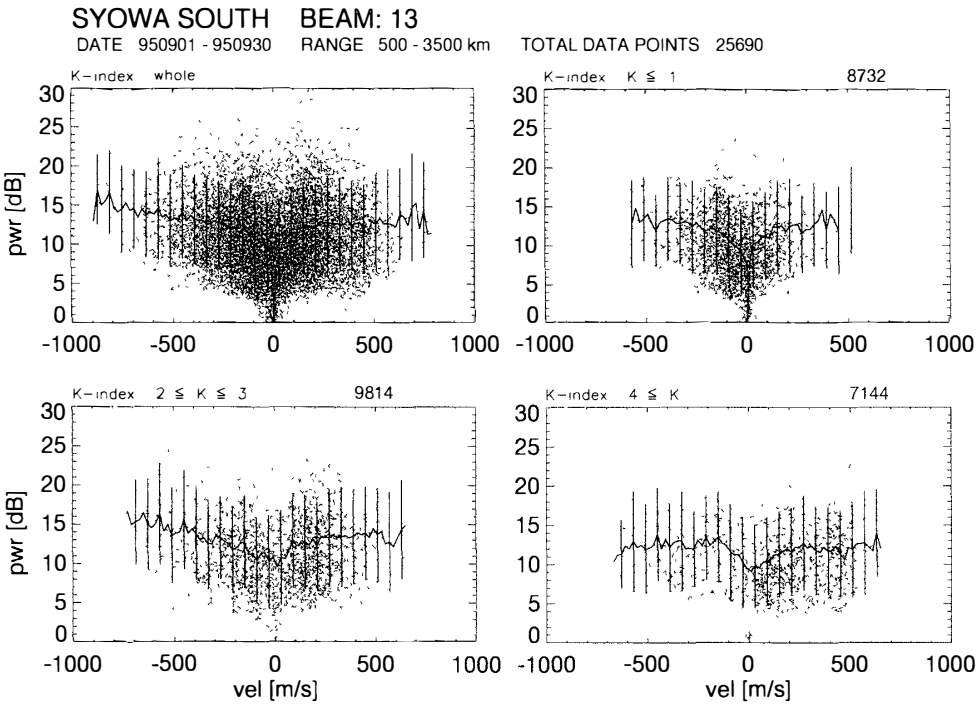

Fig. 9. Scatter plots of echo power as a function of Doppler velocity. Solid curve connects the averaged echo power in each Doppler velocity bin. Standard deviations are also indicated by vertical bars. No enough data points were available for Doppler velocities above 500 m/s.

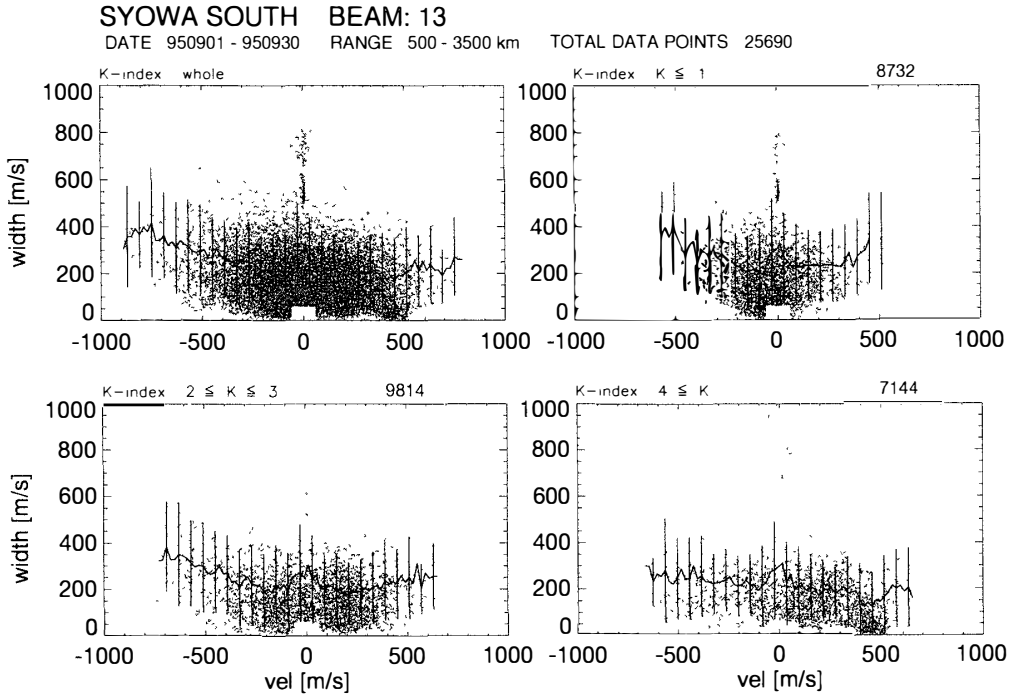

Fig. 10. Scatter plots of spectral width as a function of Doppler velocity. Standard deviations are also indicated by vertical bars. Rapid increase in spectral width at small velocities is due to elimination of ground scatter.

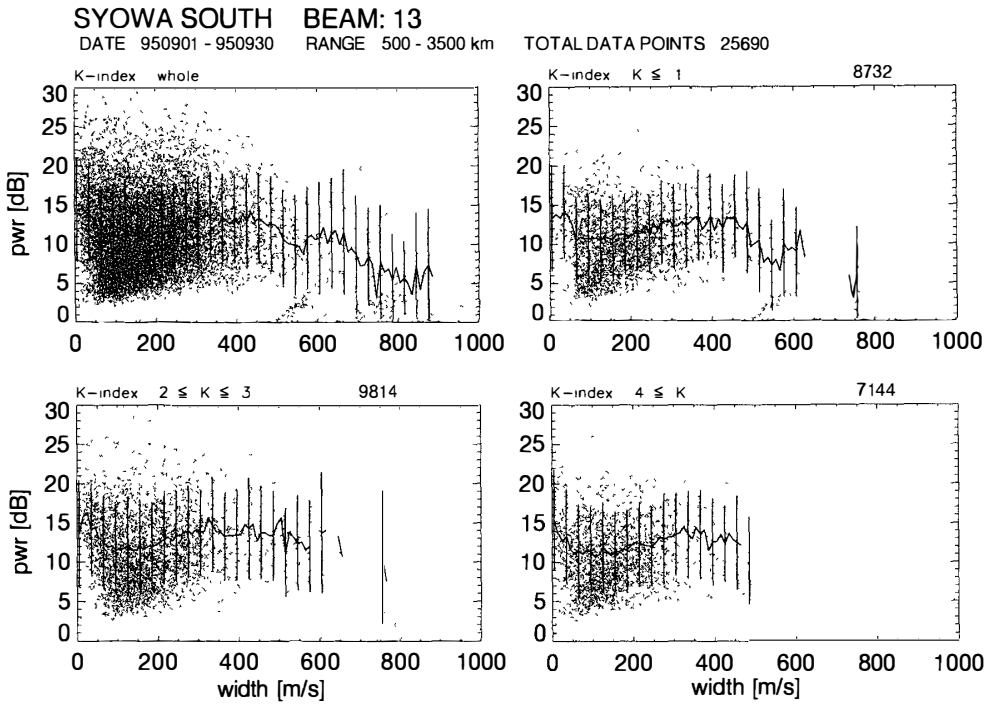

Fig. 11. Scatter plots of echo power as a function of spectral width. Standard deviations are also indicated by vertical bars. Increase in averaged echo power at small widths is due to elimination of ground scatter.

11. The solid curves with standard deviations show the averaged echo power in each spectral width bin. Note that a rapid increase in the averaged echo power at small width is due to the elimination of echoes with low spectral widths ($\leq$60 m/s) and low Doppler velocities ($\leq \pm$60 m/s). These echoes are regarded as ground scatter echoes, but may contain ionospheric echoes. Except for these data points, there is a weak positive correlation between spectral width and echo power; echo power increases with spectral width up to 500 m/s. Reasonable interpretation of this correlation has not yet been found. Qualitatively, if echo power and spectral width increase with the absolute value of Doppler velocity, echo power is expected to increase with spectral width (more discussion is given in the following section). The decrease in the averaged echo power with spectral width above 500 m/s in Fig. 11 is due both to the small amount of data points and to noise which is not excluded with our technique.

3. Discussion and Conclusion

We have presented the statistical characteristics of each parameter and the relationship between the parameters obtained with Syowa South HF radar. The most important finding is the positive correlation between the absolute value of Doppler velocity and echo power as shown in Fig. 9. This correlation can be interpreted in terms of the gradient-drift instability (*e.g.*, TSUNODA, 1988; KESKINEN and OSSAKOW, 1983). The growth rate of the gradient-drift instability depends on both electric field and plasma density gradient. If the electric field is stronger, the growth rate becomes higher, that

is, the irregularity amplitude of plasma density fluctuation grows faster and attains at higher level. Backscattered echo power of an HF radar depends on irregularity cross-section, that is, mean level of density fluctuations (HANUISE *et al.*, 1991). Since the plasma velocity in the F-region is given by $\vec{V}_E=\vec{E}\times\vec{B}/B^2$, the absolute value of Doppler velocity is proportional to the electric field strength. Therefore, the mean level of density fluctuations produced by the gradient-drift instability is expected to increase with increasing plasma velocity, resulting in stronger echo power. This is consistent with current observations. There are still large scatter in the relationship in Fig. 9. This may come from our one-dimensional (line-of-sight) observations of the Doppler velocity; actual horizontal plasma velocity is higher than the observed values. In order to resolve this problem, two-dimensional observations of plasma velocity are highly necessary. The correlations between the Doppler velocity and spectral width and those between the spectral width and echo power are not interpreted appropriately.

For the E-region gradient-drift instability, the electron density fluctuation level ($I^{1/2}$) depends theoretically on electron drift velocity (V_d) as $I\propto V_d^{2/3}$ (*e.g.*, FARLEY, 1985). This dependence has been measured and found to be rather stronger, that is, $I\propto V_d^n$ with $2\leq n\leq 3$ (HALDOUPIS *et al.*, 1998). FARLEY (1985) also predicts a relation between spectral width (W) and V_d as $W\propto V_d^{4/3}$. Unfortunately, there exist no theoretical nonlinear studies of the F-region gradient-drift instability to be compared with our observational results. Nevertheless, if we assume there is an analogy between the E-region and the F-region, spectral width W depends on Doppler velocity V by $W\propto V^m$ ($m>0$), and echo power P depends on Doppler velocity by $P\propto V^n$ ($n>0$), as shown in Fig. 9. By combining $V\propto W^{1/m}$ and $P\propto V^n$, we obtain $P\propto W^{n/m}$ which suggests a positive correlation as shown in Fig. 11.

In order to study the physical properties of the F-region HF radar echoes, we need more detailed analysis, such as classification of data by MLT and geomagnetic latitude. This kind of analysis will be useful for the discussion of other possible mechanisms for generating F-region irregularities, such as current-convective instability (*e.g.*, TSUNODA, 1988). This work is under way using larger amount of data obtained with the Syowa East HF radar in 1997.

Acknowledgments

We would like to thank all the staff who contributed to the HF radar project at Syowa Station, Antarctica.

References

BAKER, K.B., DUDENEY, J.R., GREENWALD, R.A., PINNOCK, M., NEWELL, P.T., RODGER, A.S., MARTIN, N. and MENG, C.-I. (1995): HF radar signatures of the cusp and low-latitude boundary layer. J. Geophys. Res., **100**, 7671–7695.

GREENWALD, R.A., BAKER, K.B., HUTCHINS, R.A. and HANUISE, C. (1985): An HF phased-array radar for studying small-scale structure in the high-latitude ionosphere. Radio Sci., **20** 63–79.

FARLEY, D.T. (1985): Theory of equatorial electrojet plasma waves: new developments and current status. J. Atmos. Terr. Phys., **47**, 729–744.

HALDOUPIS, C., BOURDILLON, A., DELLOUE, J. and HUSSEY, G. (1998): Wavelength dependence of Doppler

spectrum broadening in midlatitude *E* region coherent backscatter. J. Geophys. Res., **103**, 11605–11615.

HANUISE, C., VILLAIN, J.P., CERISIER, J.C., SENIOR, C., RUOHONIEMI, J.M., GREENWALD, R.A. and BAKER, K.B. (1990): Statistical study of high-latitude *E*-region Doppler spectra obtained with SHERPA HF radar. Ann. Geophys., **9**, 273–285.

HEPPNER, J.P. and MAYNARD, N.C. (1987): Empirical high-latitude electric field model. J. Geophys. Res., **92**, 4467–4489.

KESKINEN, M.J. and OSSAKOW, S.L. (1983): Theories of high-latitude ionospheric irregularities: A review. Radio Sci., **18**, 1077–1091.

NISHITANI, N., OGAWA, T., SATO, N., YAMAGISHI, H., YUKIMATTU, A.S. and WATANABE, M. (1997): Averaged pattern of ionospheric echo region and convection: Initial results from the Syowa Station HF radar. Proc. NIPR Symp. Upper Atmos. Phys., **10**, 42–49.

OGAWA, T. and IGARASHI, K. (1982): VHF radar observation of auroral *E*-region irregularities associated with moving-arcs. Mem. Natl Inst. Polar Res., Spec., **22**, 125–139.

RUOHONIEMI, J.M. and GREENWALD, R.A. (1996): Statistical patterns of high-latitude convection obtained from Goose Bay HF radar observations. J. Geophys. Res., **101**, 21743–21763.

RUOHONIEMI, J.M. and GREENWALD, R.A. (1997): Rates of scattering occurrence in routine HF radar observations during solar cycle maximum. Radio Sci., **32**, 1051–1070.

TSUNODA, R.T. (1988): High-latitude *F*-region irregularities: A review and synthesis. Rev. Geophys., **26**, 719–760.

(Received January 12, 1999; Revised manuscript accepted March 12, 1999)